

**This document is the Accepted Manuscript version of a Published Work that appeared in final form in The Journal of Physical Chemistry C, © 2016 American Chemical Society after peer review and technical editing by the publisher.**

**To access the final edited and published work is available online at:**  
**<https://doi.org/10.1021/acs.jpcc.5b10703>**

## Surface Modification of TiO<sub>2</sub> with Ag Nanoparticles and CuO Nanoclusters for Application in Photocatalysis

Maria Guadalupe Mendez Medrano, Ewa Katarzyna Kowalska, Anais Lehoux, Alexandre Herissan, Bunsho Ohtani, Daniel Bahena Uribe, Christophe Colbeau-Justin, Jose Luis Rodriguez Lopez, Hynd Remita, and Valérie Briois

*J. Phys. Chem. C*, **Just Accepted Manuscript** • DOI: 10.1021/acs.jpcc.5b10703 • Publication Date (Web): 15 Feb 2016

Downloaded from <http://pubs.acs.org> on February 19, 2016

### Just Accepted

“Just Accepted” manuscripts have been peer-reviewed and accepted for publication. They are posted online prior to technical editing, formatting for publication and author proofing. The American Chemical Society provides “Just Accepted” as a free service to the research community to expedite the dissemination of scientific material as soon as possible after acceptance. “Just Accepted” manuscripts appear in full in PDF format accompanied by an HTML abstract. “Just Accepted” manuscripts have been fully peer reviewed, but should not be considered the official version of record. They are accessible to all readers and citable by the Digital Object Identifier (DOI®). “Just Accepted” is an optional service offered to authors. Therefore, the “Just Accepted” Web site may not include all articles that will be published in the journal. After a manuscript is technically edited and formatted, it will be removed from the “Just Accepted” Web site and published as an ASAP article. Note that technical editing may introduce minor changes to the manuscript text and/or graphics which could affect content, and all legal disclaimers and ethical guidelines that apply to the journal pertain. ACS cannot be held responsible for errors or consequences arising from the use of information contained in these “Just Accepted” manuscripts.

# Surface Modification of TiO<sub>2</sub> with Ag Nanoparticles and CuO Nanoclusters for Application in Photocatalysis

M.G. Méndez-Medrano,<sup>a,b</sup> E. Kowalska,<sup>c</sup> A. Lehoux,<sup>c</sup> A. Herissan,<sup>b</sup> B. Ohtani,<sup>c</sup> D. Bahena,<sup>d</sup>  
V. Briois,<sup>e</sup> C. Colbeau-Justin,<sup>a</sup> J.L. Rodríguez-López,<sup>b</sup> and H. Remita.<sup>a,f\*</sup>

<sup>a</sup>Laboratoire de Chimie Physique, UMR 8000 CNRS, Université Paris-Sud, Université Paris-Saclay 91405 Orsay, France.

<sup>b</sup>Advanced Materials Department, IPICYT, 78216 San Luis Potosi, SLP, Mexico.

<sup>c</sup>Institute for Catalysis, Hokkaido University, North 21, West 10, 001-0021 Sapporo, Japan.

<sup>d</sup>Centro de Investigacion y de Estudios Avanzados del Instituto Politecnico Nacional, 107360, D.F., Mexico.

<sup>e</sup>Synchrotron Soleil, L'Orme des Merisiers, Saint-Aubin, BP 48, 91192 Gif-sur-Yvette Cedex - France

<sup>f</sup>CNRS, Laboratoire de Chimie Physique, UMR 8000, 91405 Orsay, France.

Email: [hynd.remita@u-psud.fr](mailto:hynd.remita@u-psud.fr); Fax : +33 (0)1 69 15 30 55; Tel: +33 (0)1 69 15 72 58.

## Abstract

Ag and CuO nanoparticles (NPs) synthesized on the surface of commercial TiO<sub>2</sub> (P25) by radiolytic reduction were characterized by Diffuse Reflectance Spectroscopy (DRS), Transmission Electron Microscopy (TEM), High Angle Annular Dark Field

1  
2  
3 Scanning Transmission Electron Microscopy (HAADF-STEM), Energy-Dispersive X-ray  
4 Spectroscopy (EDS), X-ray Photoelectron Spectroscopy (XPS) and X-ray Absorption  
5 Spectroscopy (XAS). In case of modification with silver and copper, results from HAADF-  
6 STEM, EDS, XPS and XAS show that Ag@CuO nanoparticles (large silver cores  
7 decorated with small clusters of CuO) were obtained on TiO<sub>2</sub>-P25. The photocatalytic  
8 properties of bare and modified TiO<sub>2</sub>-P25 were studied for phenol photodegradation and for  
9 acetic acid oxidation under UV and visible irradiation. The mechanisms involved in  
10 photocatalysis were studied by Time Resolved Microwave Conductivity (TRMC) and  
11 Action Spectra (AS). The electronic properties of the surface modified TiO<sub>2</sub>-P25 were  
12 studied by TRMC to follow the charge-carrier dynamics. The modification with the Ag  
13 nanoparticles or CuO nanoclusters induces an increase in the photocatalytic activity under  
14 both UV and visible light. The photocatalytic activity of Ag@CuO/P25 is higher under UV  
15 light, but lower under visible light compared to the activity of CuO/P25 and Ag/P25.  
16 TRMC measurements show that surface modification of TiO<sub>2</sub>-P25 with Ag, CuO and  
17 Ag@CuO nanoparticles plays a role in charge-carrier separation, increasing the activity  
18 under UV-light, and that Ag@CuO NPs are more efficient electron scavengers than Ag  
19 NPs and CuO nanoclusters. The Localized Surface Plasmon Resonance (LSPR) of Ag NPs  
20 and the narrow band-gap of CuO induce an activity under visible light. The TRMC shows  
21 also responses under visible light irradiation at different fixed wavelengths indicating that  
22 electrons are injected from Ag NPs in the conduction band (CB) of TiO<sub>2</sub>-P25. Moreover,  
23 under visible light, the photocatalytic activity of CuO/P25 is higher than that of plasmonic  
24 Ag/P25. CuO is able to activate TiO<sub>2</sub>-P25 in a wider range of wavelengths under visible  
25 light irradiation, compared to the activation achieved by the presence of silver. The action  
26 spectra correlate with the absorption spectra for irradiation wavelengths in the range of  
27  
28  
29  
30  
31  
32  
33  
34  
35  
36  
37  
38  
39  
40  
41  
42  
43  
44  
45  
46  
47  
48  
49  
50  
51  
52  
53  
54  
55  
56  
57  
58  
59  
60

350-470 nm proving that decomposition of acetic acid is carried out by a photocatalytic mechanism.

## 1. Introduction

In the past decades, a lot of research has been done to develop new, efficient and cheap technologies for the development of wastewater treatment using solar irradiation, and one interesting option opened lately, is the so-called plasmonic photocatalysts, which consist of semiconductors (SCs) modified with plasmonic metal nanoparticles (MNPs) on their surface.<sup>1</sup> In this sense, titanium dioxide (TiO<sub>2</sub>) is the most investigated and used SC because of its high photocatalytic activity, stability, low cost and non-toxicity. The increasing interest in the development of plasmonic photocatalysts is due to the enhanced photoactivity that they show, since MNPs can work as electron pool or electron donors under UV and visible light, respectively. Furthermore, the MNPs present localized surface plasmon resonance (LSPR), which is a special and unique feature responsible for the activation of the photocatalyst under visible light.<sup>1,2,3</sup>

It has been widely reported that surface modification of TiO<sub>2</sub> with metal NPs could improve its photocatalytic activity, especially with noble metals such as Pt, Pd, Cu, Ag and Au.<sup>4,5,6,7,8,9</sup> However, there are only few works focused on the modification of TiO<sub>2</sub> or other substrates with Cu.<sup>7,8,10</sup> For example, Qiu *et al.* reported that Cu(II) clusters, grafted on the surface of SC with narrow band-gap ((Sr<sub>1-y</sub>Na<sub>y</sub>)(Ti<sub>1-x</sub>Mo<sub>x</sub>)O<sub>3</sub>), acted as a co-catalyst to efficiently reduce oxygen molecules (multi-electron reduction).<sup>11</sup> Moreover, coupling of TiO<sub>2</sub> (n-type SC) with

1  
2  
3 narrow band-gap semiconductors such as CuO (p-type SC) is another strategy to  
4  
5 obtain visible light active photocatalysts.<sup>12,13</sup>  
6  
7

8 Silver NPs are extremely attractive because of their high catalytic activity,  
9  
10 widespread optical properties (size- and shape-dependent), antimicrobial properties,  
11  
12 and potential applications in biological and chemical sensing, based on phenomena  
13  
14 of Surface-Enhanced Raman Scattering (SERS), LSPR, and Metal-Enhanced  
15  
16 Fluorescence (MEF).<sup>6</sup> In addition, modification of TiO<sub>2</sub> with silver NPs results in  
17  
18 enhanced photocatalytic activity under both UV and visible light irradiation and  
19  
20 improved anti-bacterial properties.<sup>6,14,15</sup>  
21  
22  
23

24 However, the use of Cu, in agreement with Irie *et al.*,<sup>16</sup> is more desirable due to its  
25  
26 low cost and excellent catalytic and antifungal properties. It has recently been  
27  
28 reported that surface modification of TiO<sub>2</sub> with bimetallic Ag-Cu nanoparticles leads  
29  
30 to enhancement of the photocatalytic activity of TiO<sub>2</sub> for CO<sub>2</sub> reduction compared to  
31  
32 its modification with monometallic NPs.<sup>17</sup>  
33  
34  
35

36 In this work, we present synthesis of Ag nanoparticles and/or CuO nanoclusters  
37  
38 by radiolysis on commercial TiO<sub>2</sub>-P25. The photocatalytic activity of these  
39  
40 photocatalysts has been investigated for photooxidation reactions of phenol and  
41  
42 acetic acid. Time Resolved Microwave Conductivity (TRMC) has been used to study  
43  
44 charge-carrier dynamics. The aim of this study was to correlate the photocatalytic  
45  
46 activity of modified TiO<sub>2</sub>-P25 with Ag nanoparticles and CuO nanoclusters with the  
47  
48 AS and TRMC signals obtained at different excitation wavelengths to understand the  
49  
50 mechanisms involved in the photocatalytic process under UV and visible light.  
51  
52  
53  
54  
55  
56  
57  
58  
59  
60

## 2. Experimental

### 2.1. Materials

Commercial titanium(IV) oxide P25 (TiO<sub>2</sub>-P25, Evonik, surface area of ca. 50 m<sup>2</sup> g<sup>-1</sup>), composed of a mixture of the crystalline phases: anatase (73-85%), rutile (14-17%) and amorphous titania (0-13%),<sup>18</sup> was used as a support material. Silver sulfate (Ag<sub>2</sub>SO<sub>4</sub>, Fulka, purity ≥ 99.4%) and cupric sulfate (CuSO<sub>4</sub>, Sigma, purity ≈ 99%) were used as metal precursors. Other used chemicals were deionized water (Milli-Q with 18.6 MΩ), methanol (CH<sub>3</sub>OH, ACS reagent, ≥ 99.8%), phenol (C<sub>6</sub>H<sub>5</sub>OH, Fulka), 2-propanol (CH<sub>3</sub>CH(OH)CH<sub>3</sub>, Sigma-Aldrich, 99.5%), and acetic acid (CH<sub>3</sub>COOH, Wako, 99.7%).

### 2.2. Photocatalyst Preparation: Modification of P25 by Radiolysis

Ag<sup>+</sup> and/or Cu<sup>2+</sup> ions were reduced by radiolysis on TiO<sub>2</sub>-P25 surface. Aqueous solutions (with 0.1-M 2-propanol, used as scavenger of OH<sup>•</sup> radicals generated by water radiolysis)<sup>19</sup> containing Ag<sub>2</sub>SO<sub>4</sub>, CuSO<sub>4</sub> or a mixture of Ag<sub>2</sub>SO<sub>4</sub> and CuSO<sub>4</sub> (the total concentration in salt being 1x10<sup>-3</sup> M) were put in contact with TiO<sub>2</sub>-P25 (the loading of Cu or Ag metal was 0.5 wt%). The samples were labeled as P25, Ag/P25 and CuO/P25. For the suspensions containing a mixture of Ag<sup>+</sup> and Cu<sup>2+</sup>, different molar ratios of Ag:Cu were used, *i.e.* 1:1, 1:3, and 3:1, keeping the total nominal metal content at 1 wt%. The resulting modified catalysts were respectively labeled as Ag@CuO1:1/P25, Ag@CuO1:3/P25, Ag@CuO3:1/P25.

The suspensions were first sonicated for 3 minutes, deaerated with nitrogen (under stirring) and then irradiated with a <sup>60</sup>Co panoramic gamma source (dose rate = 2.3 kGy h<sup>-1</sup>) for 3.5 h. The silver and copper ions were reduced by the solvated

1  
2  
3 electrons and the alcohol radicals induced by solvent radiolysis. The applied dose is  
4  
5 sufficient to reduce all the metal ions into their zero valency. The modified TiO<sub>2</sub>-P25  
6  
7 photocatalysts were separated by centrifugation and dried at 60°C for 18 h. The  
8  
9 supernatant was completely transparent after centrifugation, indicating that all the  
10  
11 Ag and Cu-based NPs were deposited on TiO<sub>2</sub>-P25.<sup>19,20</sup>  
12  
13

### 14 15 **2.3. Materials Characterization**

16  
17 For the Transmission Electron Microscopy (TEM) observations, the samples were  
18  
19 dispersed in 2-propanol in an ultrasonic bath for few minutes and then, one drop of  
20  
21 the suspension was deposited on a gold coated holey carbon grids (SPI method). The  
22  
23 samples were characterized by High Angle Annular Dark Field Scanning  
24  
25 Transmission Electron Microscopy (HAADF-STEM). The HAADF-STEM images  
26  
27 were recorded using C<sub>s</sub> corrected JEOL-ARM-200F electron transmission  
28  
29 microscope at 200 kV. The HAADF-STEM images were acquired with a camera  
30  
31 length of 8 cm and the collection angles of 70-280 mrad.  
32  
33  
34

35  
36 Energy-Dispersive X-ray Spectroscopy (EDS) measurements for line scan profiles  
37  
38 and mapping were obtained with a solid state detector from Oxford with an 80 mm<sup>2</sup>  
39  
40 window. X-ray Photoelectron Spectroscopy (XPS) characterization was conducted  
41  
42 on a JEOL JPS-9010MC with a hemispherical electron energy analyzer, using Mg  
43  
44 K $\alpha$  radiation. The samples were mounted on carbon films, each carbon film was  
45  
46 fully covered with the sample in order to avoid powder release. After overnight  
47  
48 degassing in the preparation chamber, the samples were inserted in the analysis  
49  
50 chamber with a pressure lower than 10<sup>-7</sup> torr. High resolution scans were taken for  
51  
52 five elements, and number of scans differed depending on each element content in  
53  
54 the sample, i.e., 50 scans were taken for Ti and O, 100 scans for C and 300-500  
55  
56  
57  
58  
59  
60

1  
2  
3 scans for Ag and Cu. Diffuse Reflectance Spectroscopy (DRS) was recorded with a  
4  
5 UV-Vis-NIR spectrophotometer, model Cary 5000 Series from Agilent  
6  
7 Technologies, equipped with an integrating sphere for diffuse and total reflection  
8  
9 measurements and using a KBr reference sample.  
10

11  
12 Cu K-edge XANES measurements were carried out at the SAMBA beamline  
13  
14 (SOLEIL, Saint-Aubin) using a Si(220) fixed-exit double crystal monochromator.  
15  
16 Harmonic rejection was done by two Pd coated mirrors at 5.5 mrad grazing  
17  
18 incidence. Measurements were done on pellets of samples at room temperature in  
19  
20 fluorescence mode using a Ge 35 pixel-array detector.  
21  
22

23  
24 Time Resolved Microwave Conductivity (TRMC) method was used to study the  
25  
26 dynamics of photogenerated charge-carriers under UV and visible irradiation. A  
27  
28 pulsed laser source with an optical parametric oscillator (OPO) EKSPLA, NT342B,  
29  
30 tunable in the range between 220–2000 nm was used for TRMC measurements. The  
31  
32 full width at half-maximum (FWHM) of one pulse was 8 ns with repetition  
33  
34 frequency of the pulses at 10 Hz, and microwaves generated by a Gunn diode (30  
35  
36 GHz). Several wavelengths were used, 355, 400, 450, 470, 480, 550, 600, and 650  
37  
38 nm, and the corresponding laser energies were 1.7, 0.9, 6.7, 6.2, 5.8, 4.5, 2.5, and 1.7  
39  
40 mJ cm<sup>-2</sup> respectively.  
41  
42  
43  
44

45  
46 The principle of this technique was described in previous papers.<sup>5,7,21,22</sup> In brief,  
47  
48 TRMC consists in the measurement of the microwave power reflected by a semi-  
49  
50 conductor sample during illumination by a nanosecond pulsed laser. The signal  
51  
52 obtained by the diode detector is transformed into voltage for input to the  
53  
54 oscilloscope. The difference between the incident and the reflected microwave  
55  
56  
57  
58  
59  
60

1  
2  
3 power gives the absorbed microwave power by the sample, which is directly  
4  
5 proportional to the conductivity of the sample.  
6  
7

8 The main data provided by TRMC are given by (a) the maximum value of the  
9  
10 signal ( $I_{\max}$ ), which reflects the number of the excess charge-carriers created by the  
11  
12 pulse, weighted by the mobility of the charge-carriers and by the influence of  
13  
14 charge-carrier decay processes during the excitation, and (b) the decay of the signal  
15  
16  $I(t)$ , which is due to the decrease of the excess electrons controlled by recombination  
17  
18 and trapping.<sup>21,23</sup>  
19  
20

## 21 22 **2.4 Photocatalytic Activity Tests**

### 23 24 *2.4.1. Phenol Degradation under UV and Visible Light*

25  
26 The photocatalytic activity of the modified photocatalysts was tested for  
27  
28 photodecomposition of phenol ( $C_6H_5OH$ ), used as model pollutant in water (50  
29  
30 ppm), under UV and visible illumination. The photodegradation was carried out in a  
31  
32 10-mm light path quartz cell reactor containing 3.5 mL of the phenol solution and 1  
33  
34  $g\ L^{-1}$  of photocatalyst. Before irradiation, the photocatalyst was dispersed in the  
35  
36 solution by sonication for 30 seconds, and then by magnetic stirring for 10 minutes  
37  
38 in the dark to reach the equilibrium between adsorption and desorption. Then, the  
39  
40 solution was irradiated using a xenon lamp (Oriel 300W) with or without cut-off  
41  
42 filter (AM-32603-1, LOT-Oriel) for experiments carried out under visible light ( $\lambda >$   
43  
44 450 nm) or UV irradiation, respectively. The photocatalytic tests were conducted  
45  
46  
47  
48  
49  
50  
51 under oxygen bubbling at a fixed rate flow.

52  
53 Aliquots of 0.5 mL were sampled from the reactor at different time intervals. The  
54  
55 powder was separated by centrifugation and then the resultant transparent solution  
56  
57 was analyzed by High Performance Liquid Chromatography (HPLC, Agilent 1260  
58  
59  
60

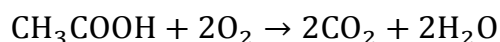
1  
2  
3 infinity quaternary LC) equipped with a UV-detector set at 260 nm for phenol  
4  
5 analysis. The column was an adsorbosphere C18 in reverse phase (5  $\mu\text{m}$ , I = 150  
6  
7 mm, ID = 4.6 mm, Alltech) combined with an All-Guard cartridge system TM  
8  
9 (7.5x4.6 mm, Alltech) for elution at 1-mL  $\text{min}^{-1}$  flow rate. An isocratic mobile phase  
10  
11 consisted of 80%  $\text{H}_2\text{O}$  and 20% acetonitrile (ACN). Star software was applied for  
12  
13 data analysis.  
14  
15

#### 16 17 18 *2.4.2. Acetic Acid Degradation-Action Spectrum*

19  
20 The photocatalytic degradation of acetic acid was carried out for 30 mg of  
21  
22 photocatalyst suspended in 3 mL of an aqueous solution of acetic acid (5 v%), inside  
23  
24 quartz cells with a volume of ca. 12 mL. The cells were sealed with a septum to  
25  
26 avoid the leakage of generated  $\text{CO}_2$ . The suspensions were stirred in the dark for 10  
27  
28 min (to attain the adsorption equilibrium). The illumination with a 300-W xenon  
29  
30 lamp (Hamamatsu Photonics C2578-02) equipped with a diffraction grating type  
31  
32 illuminator (Jasco CRM-FD) allowed the selection of the irradiation wavelength in  
33  
34 the range between 350–680 nm, with a step of 30 nm. The samples were irradiated  
35  
36 with a monochromatic light with a full-width at half-maximum (FWHM) of 15 nm  
37  
38 irrespective of the selected wavelength, and the intensity of irradiation ( $1.24\text{--}3.9 \times 10^8$   
39  
40  $\text{Einstein s}^{-1}$ ), measured by a Hioki 3664 optical power meter was maintained at ca.  
41  
42 3.5 mW.  
43  
44  
45  
46  
47

48 The samples were irradiated for 90 min under stirring. Every 30 min, a 0.2 mL of  
49  
50 gas sample was taken with a syringe from the quartz cell and generated  $\text{CO}_2$  was  
51  
52 analyzed with a gas chromatograph (Shimadzu GC-14B) equipped with a flame  
53  
54 ionization detector (FID). The sensitivity of a FID detector was enhanced by  
55  
56  
57  
58  
59  
60

1  
2  
3 converting of carbon dioxide into methane in an in-line methanizer (Shimadzu  
4 MTN-1). The reaction of acetic acid degradation is the following:<sup>9</sup>  
5  
6



7  
8  
9  
10 The apparent quantum efficiency was calculated as the rate of CO<sub>2</sub> evolution from  
11 the decomposition of acetic acid versus the flux of incident photons, assuming that  
12 four photons were required.  
13  
14

15  
16  
17 In this article, we studied the surface modified TiO<sub>2</sub>-P25 with Ag, CuO, and  
18 Ag@CuO with different Ag:Cu ratios. The results and figures corresponding to  
19 Ag/P25, CuO/P25 and Ag@CuO1:1/P25 are presented in the main article, while the  
20 results for other Ag:Cu ratios (1:3 and 3:1) are mainly shown in *Supporting*  
21 *Information*.  
22  
23  
24  
25  
26  
27  
28  
29  
30  
31

### 32 **3. Results and Discussion**

#### 33 **3.1. Radiolytic synthesis**

34  
35  
36 Ag<sup>+</sup> and Cu<sup>2+</sup> were reduced on TiO<sub>2</sub>-P25 by solvated electrons and reducing  
37 (CH<sub>3</sub>)<sub>2</sub>C<sup>•</sup>OH radicals induced by radiolysis. It is well known that high energy  
38 radiation (γ-rays, X-rays, electrons or ions beams) of water leads to the formation of  
39 free radicals such as solvated electrons (e<sup>-</sup><sub>s</sub>) (which are strong reducing species  
40 (E<sup>0</sup>(H<sub>2</sub>O/e<sup>-</sup><sub>s</sub>) = -2.87 V<sub>NHE</sub>)), H<sup>•</sup> (E<sup>0</sup>(H<sup>+</sup>/H<sup>•</sup>) = -2.3 V<sub>NHE</sub>) and OH<sup>•</sup> radicals  
41 (E<sup>0</sup>(HO<sup>•</sup>/H<sub>2</sub>O) = +2.8 V<sub>NHE</sub>)).<sup>19</sup> The generated hydroxyl radicals OH<sup>•</sup> (strong oxidant  
42 species) are scavenged by addition of 2-propanol (0.1 M), which yields after  
43 reactions with OH<sup>•</sup> and H<sup>•</sup> to a secondary reducing radical (CH<sub>3</sub>)<sub>2</sub>C<sup>•</sup>OH  
44 (E<sup>0</sup>((CH<sub>3</sub>)<sub>2</sub>CO/(CH<sub>3</sub>)<sub>2</sub>C<sup>•</sup>OH) = -1.8 V<sub>NHE</sub>).<sup>19</sup> Alcohol radicals and e<sup>-</sup><sub>s</sub> are powerful  
45  
46  
47  
48  
49  
50  
51  
52  
53  
54  
55  
56  
57  
58  
59  
60

1  
2  
3 reducing agents, which are able to reduce metal ions to lower valences and finally to  
4 metal atoms. The energy deposition throughout the suspension and continuous  
5 stirring during radiation ensure homogeneous distribution of the radiolytic radicals  
6 and therefore a homogeneous reduction and nucleation leading to the formation of  
7 nanoparticles homogeneous in size.<sup>19,20</sup> The radiolytic reduction mechanisms of  
8 silver and copper ions have been already described in other publications.<sup>6,24</sup> The  
9 modified TiO<sub>2</sub>-P25 with Ag and/or Cu presented different colors (see Table 1).

10  
11  
12  
13  
14  
15  
16  
17  
18  
19  
20 **Table 1.** Characteristics of the modified photocatalysts

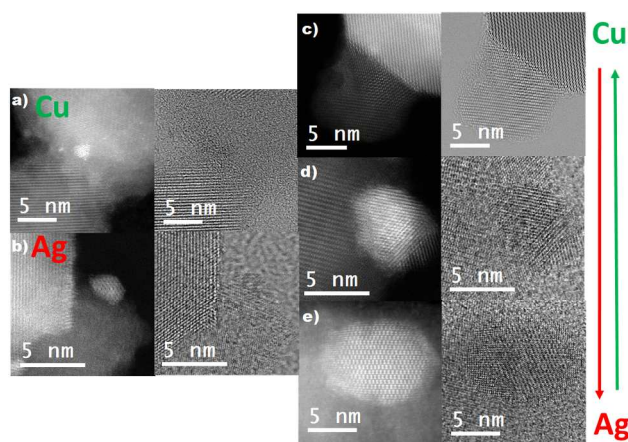
Photocatalysts	Molar ratio of AgCu	Color of sample
CuO/P25	0:1	Light-green
Ag@CuO1:3/P25	1:3	Light-yellow
Ag@CuO1:1/P25	1:1	Light-brown
Ag@CuO3:1/P25	3:1	Light-brown
Ag/P25	0:1	Light-pink

21  
22  
23  
24  
25  
26  
27  
28  
29  
30  
31 **3.2. Characterization of the Photocatalysts**

32  
33 For all the modified titania samples, TEM observations show metal nanoparticles  
34 homogeneously dispersed on TiO<sub>2</sub>-P25 surface (see Fig. S1-1). For CuO/P25 and  
35 Ag/P25 samples, small nanoparticles of around 1-2 nm were observed on the surface  
36 of TiO<sub>2</sub>-P25 (Fig. S1-2a and S1-2e). For the titania co-modified with both elements,  
37 larger nanoparticles (5-12 nm) were formed on the TiO<sub>2</sub>-P25 surface (see Fig. S1-  
38 2b-d).

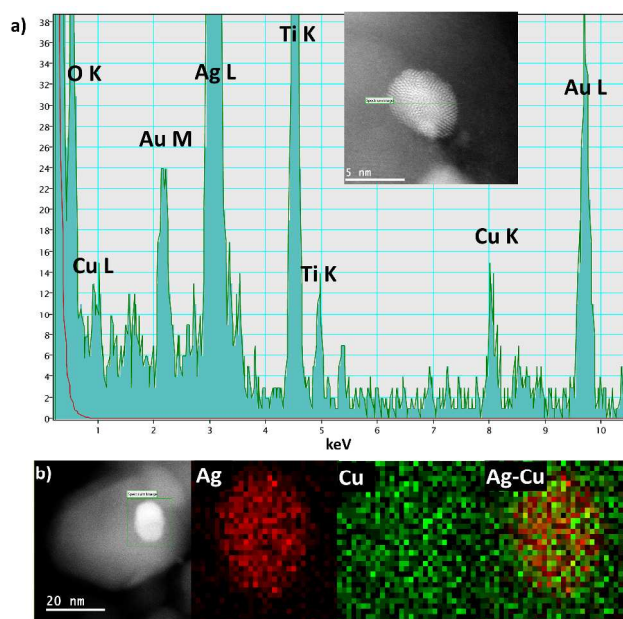
39  
40 For the titania modified with Cu and/or Ag, the HAADF-STEM images (Fig. 1)  
41 show metal nanoparticles located on the TiO<sub>2</sub>-P25 surface. Since the brightness is  
42 approximately proportional to  $Z^2$  ( $Z$  being the atomic number), any difference in  
43 brightness would reflect the presence of two different elements. Therefore, due to the  
44 atomic number difference between Ag (47) and Cu (29), the areas with higher  
45  
46  
47  
48  
49  
50  
51  
52  
53  
54  
55  
56  
57  
58  
59  
60

1  
2  
3 brightness within the NPs are attributed to columns of atoms richer in silver, and the  
4  
5 areas with lower brightness are attributed to columns richer in copper. As the  
6  
7 brightness is not regular, there is segregation between Ag and Cu. The HAADF-  
8  
9 STEM images for Ag@CuO1:3/P25 sample (Fig. 1c) show—that Ag-Cu-based  
10  
11 nanoparticles have a core-shell structure, where Ag is the core, and the Cu is the  
12  
13 shell part. A similar core-shell structure is obtained for the other Ag:Cu molar ratios,  
14  
15 *i.e.*, Ag@CuO1:1 and Ag@CuO3:1, as it can be seen in the Fig. 1d and 1e,  
16  
17 respectively. In the Ag@CuO3:1/P25 sample, the core composed of Ag covers a  
18  
19 larger area of the total particle, compared to that observed in the Ag@CuO1:3/P25  
20  
21 sample. Additionally, an image with the bright field (BF) observation mode in the  
22  
23 STEM technique is shown in the right part of Figs. 1a-e where it is possible to  
24  
25 observe different arrangements of the crystallographic planes.  
26  
27  
28  
29  
30  
31



32  
33  
34  
35  
36  
37  
38  
39  
40  
41  
42  
43  
44  
45  
46  
47 **Figure 1.** HAADF-STEM (left) and BF-STEM (right) of a) Cu/P25, b) Ag/P25, and  
48  
49 Ag@CuO systems; c) Ag@CuO1:3/P25, d) Ag@CuO1:1/P25, and e) Ag@CuO3:1/P25.  
50  
51  
52  
53  
54  
55  
56  
57  
58  
59  
60

1  
2  
3 The composition of the Ag and Cu-based NPs was investigated by EDS. Different  
4 nanoparticles were analyzed, and the profile spectra across the various individual  
5 NPs were taken (Fig. 2a. and Fig. S2). Fig. 2b shows chemical mappings for Ag and  
6 Cu-based nanoparticles. Ag (L) and Cu (L) maps clearly revealed the formation of  
7 the core(Ag)-shell(Cu) (or shell(CuO)) (composite image). Ag nanoparticles seem to  
8 be decorated on their surface by small clusters of Cu ( $\text{Cu}^0$  or Cu oxides).  
9  
10  
11  
12  
13  
14  
15  
16  
17  
18  
19  
20



21  
22  
23  
24  
25  
26  
27  
28  
29  
30  
31  
32  
33  
34  
35  
36  
37  
38  
39  
40  
41  
42  
43 **Figure 2.** a) EDS analysis and b) Elemental mapping performed at a nanoparticle of  
44 Ag@CuO1:1/P25 on P25 (Cu signal in green and Ag signal in red).  
45  
46  
47  
48  
49

50 EDS line scan signals of Ag and Cu are shown in Fig. S3. Different intensities  
51 along the different regions of the NPs are clearly observed. The HAADF-STEM  
52 images of Ag@CuO1:1/P25 show nanoparticles adsorbed on  $\text{TiO}_2$ -P25 (Fig. S3 f,  
53 left). Both the Ag-L and Cu-L peaks demonstrate non-homogeneous dispersion of  
54  
55  
56  
57  
58  
59  
60

1  
2  
3 Ag and Cu atoms where the core is richer in Ag. Therefore, the EDS line scans  
4 evidenced the core-shell structure of co-modified samples (Fig. S3 f, right). The  
5 information obtained from high resolution TEM images, HAADF-STEM and EDS  
6 analyses confirm the formation of core-shell Ag@Cu (or Ag@CuO) NPs on TiO<sub>2</sub>-  
7 P25. The Cu–Ag system has a strong tendency to phase separation, due to the large  
8 difference in the atom size ( $r_{\text{Ag}}/r_{\text{Cu}} = 1.13$ , where  $r_{\text{M}}$  is the atomic radius of metal M),  
9 and the difference in the cohesive energies between the two metals  $E_{\text{Ag}}^{\text{coh}} - E_{\text{Cu}}^{\text{coh}} =$   
10 0.55 eV (the biggest atom (Ag) being the less cohesive).<sup>25</sup> This phase segregation  
11 has already been reported for the system Ag-Cu.<sup>17,26,27,28</sup> This surface segregation of  
12 silver and copper was also studied by Monte Carlo simulations.<sup>26,28</sup> Previous studies  
13 have shown that a system at thermodynamic equilibrium possesses silver as shell  
14 around copper core.<sup>29</sup> Our system is out of equilibrium and it is suggested that silver  
15 is reduced before copper leading to Ag<sub>core</sub>-Cu<sub>shell</sub> NPs. It has also been reported that  
16 when Cu is oxidized it segregates to the surface of the system.<sup>30</sup>

17  
18  
19  
20  
21  
22  
23  
24  
25  
26  
27  
28  
29  
30  
31  
32  
33  
34  
35  
36  
37 In order to analyze the chemical composition of the modified TiO<sub>2</sub>-P25 and to  
38 identify the chemical state of Cu and Ag elements in the samples, XPS  
39 measurements were performed. It was found that samples were homogeneous  
40 because the XPS signals from different regions of the sample were very reproducible  
41 in both chemical composition and energy distribution. XPS analyses attested the  
42 metallic nature of Ag nanoparticles, as shown in Fig. 3, Fig. S4, and Tables 2 and  
43 S1. The Ti2p peaks are characteristic of Ti<sup>4+</sup> in TiO<sub>2</sub> with two main components at  
44 459.5 and 465.5 eV related to Ti2p<sub>3/2</sub> and Ti2p<sub>1/2</sub> orbitals and the O1s peaks at 530.5  
45 eV attributed to oxygen of TiO<sub>2</sub>. The Ag3d core peaks split into two components,  
46 Ag3d<sub>5/2</sub> and Ag3d<sub>3/2</sub>, due to spin-orbit coupling ( $\Delta_{\text{BE}}(\text{Ag}3\text{d}_{5/2-3/2}) = 6$  eV), and the  
47  
48  
49  
50  
51  
52  
53  
54  
55  
56  
57  
58  
59  
60

1  
2  
3 binding of the Ag3d<sub>5/2</sub> core peaks is characteristic of metallic silver.<sup>6,31,32</sup> In Fig. 3a-  
4  
5 c, the Ag-modified TiO<sub>2</sub>-P25 exhibits at the Ag3d level, two reproducible peaks  
6  
7 (around 368.3 and 374.3 eV), which are typical for the 3d<sub>5/2</sub>/3d<sub>3/2</sub> spin-orbit splitting  
8  
9 of Ag. The Ag 3d<sub>5/2</sub> binding energy at peak maximum 368.3 eV corresponds to the  
10  
11 value reported for metallic Ag.<sup>6,32,33,34</sup> However, the broadening of the peak width is  
12  
13 noticed when compared to that of pure metal for the same recording conditions. This  
14  
15 feature is due to additional contributions associated to other chemical Ag  
16  
17 environment. The small additional peaks at higher binding energy localized at 368.6  
18  
19 eV and 374.6 eV cannot be related to silver oxides (which are known to present a  
20  
21 positive shift in the binding energy),<sup>6,33,34,35</sup> and they may correspond to the  
22  
23 interaction of Ag NPs with the TiO<sub>2</sub> substrate as it has been previously reported.<sup>6</sup>  
24  
25  
26  
27  
28

29 In the same way, two components Cu2p<sub>3/2</sub> and Cu2p<sub>1/2</sub> are observed for the Cu  
30  
31 core peaks.<sup>36,37</sup> In Fig. 3b-d, the BE positions of Cu2p<sub>3/2</sub> core levels are in the range  
32  
33 of 933.3 - 933.4 eV. These positions are closer to the positions of CuO (Cu<sup>II</sup>),<sup>36,38</sup>  
34  
35 rather than Cu<sup>0</sup>, however the satellite peak characteristic of CuO (or Cu<sup>II</sup>) is not  
36  
37 observed or is very weak, and this behavior is presented in all the samples containing  
38  
39 Cu (Figs. 3a-d and S4-1). It has to be noted that the positions of the XPS peaks are  
40  
41 sensitive to the cluster size, especially for very small clusters (size < 3 nm).<sup>39,40</sup>  
42  
43 Chusue *et al.* reported that the XPS shake-up is sensitive to the CuO particle size,  
44  
45 and this satellite decreases with the reduction state of Cu, but also with the decrease  
46  
47 of the particle size.<sup>40</sup>  
48  
49  
50  
51  
52  
53  
54  
55  
56  
57  
58  
59  
60

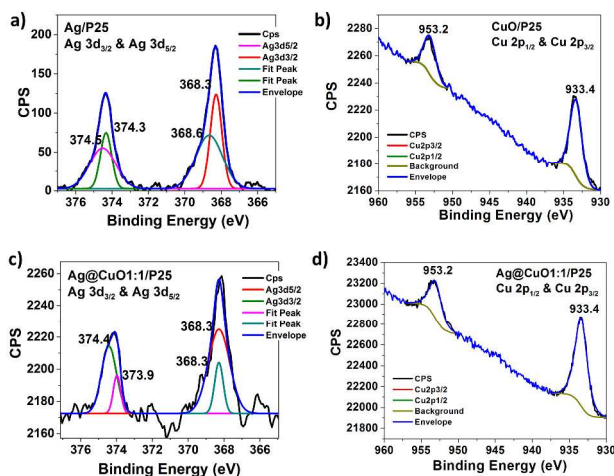


**Figure 3.** XPS spectra for a) Ag 3d and c), b) and d) Cu 2p of Ag/P25, Ag@CuO1:1/P25, CuO/P25 samples.

**Table 2.** Binding energies of CuO/P25, Ag/P25 and Ag@CuO1:1/P25 samples determined by XPS showing the binding energies of Ag-3d, Cu-2p, Ti-2p, O-1s

Samples	Ag		Cu		Ti		O
	3d <sub>3/2</sub>	3d <sub>5/2</sub>	2p <sub>1/2</sub>	2p <sub>3/2</sub>	2p <sub>1/2</sub>	2p <sub>3/2</sub>	1s
	[eV]						
CuO/P25	-	-	953.2	933.4	465.5	459.5	530.8
Ag@CuO1:1/P25	374.4	368.3	953.2	933.4	465.8	459.9	531.3
Ag/P25	374.3	368.3	-	-	465.3	459.4	530.6

Therefore, Cu K-edge XANES spectra were measured in order to corroborate the oxidation states of Cu deduced from XPS. It has been found, that the energy position of the rising edge of the spectra and shape of white line for all the TiO<sub>2</sub>-P25 modified with copper (Cu alone or associated with Ag) are characteristic of Cu<sup>II</sup> species,<sup>41</sup> as shown in Fig. 4.

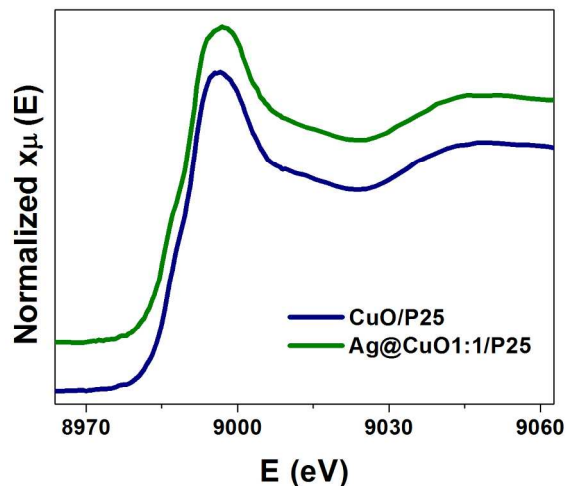


**Figure 4.** Cu K-edge XAS spectra for CuO/P25 and Ag@CuO1:1/P25 samples.

Solvated electrons induced by radiolysis are very strong reducing species able to reduce non noble metals, which are difficult to reduce by chemical methods.<sup>20,24,42</sup> Silver and copper ions are reduced on TiO<sub>2</sub>-P25 by solvated electrons and alcohol radicals.<sup>6,24</sup> However, copper clusters are sensitive to oxygen and are most probably very fast oxidized in air. Thus, the Ag<sub>core</sub>-Cu<sub>shell</sub> nanoparticles turn into Ag@CuO in air. Fig. 5a shows an aberration corrected HAADF-STEM image of Ag@CuO(1:1)/P25 sample allowing to distinguish two different elements, *i.e.*, Ag and Cu, based on the brightness of the image. Accordingly, as well as results from XPS and XAS, a representative scheme of this core-shell structure on the TiO<sub>2</sub>-P25 surface is depicted in Fig. 5b.

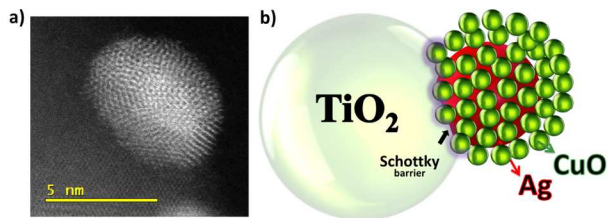


**Figure 5.** a) Representative aberration corrected STEM-HAADF image for an Ag@CuO1:1 particle supported on TiO<sub>2</sub>-P25, showing Ag-NPs covered with an ensemble of CuO clusters, and b) A schematic morphology of the modified TiO<sub>2</sub>-P25 with Ag-CuO nanoparticles.

The optical properties of the modified TiO<sub>2</sub>-P25 were studied by DRS. Fig. 6 and Fig. S5 show the spectra of bare and modified TiO<sub>2</sub>-P25. The spectrum of TiO<sub>2</sub>-P25 shows an absorption edge at around 400 nm due to the presence of rutile.<sup>43</sup> The DRS spectra of the modified samples exhibit a slight shift in the absorption to longer wavelengths for all surface-modified photocatalysts. This effect has already been reported for TiO<sub>2</sub> modified with Pt, Pd, Ag, and Au-Cu,<sup>4,5,6,7,8</sup> and could be attributed to stabilization of the CB of TiO<sub>2</sub>-P25 by the interaction with the Ag NPs and CuO nanoclusters. The modified samples absorb in the visible and near infra-red (IR) region, while bare TiO<sub>2</sub>-P25 does not. Note that absorption with a maximum at 510 nm was obtained with Ag/P25 while a large absorption band with a maximum at 800 nm was observed for CuO/P25.

These absorptions result in pink and yellow colors of the modified TiO<sub>2</sub>-P25 samples. TiO<sub>2</sub>-P25 co-modified with Ag and CuO absorbs in the visible and near IR. The maximum absorption in the visible region is respectively at 480 nm for Ag@CuO1:3/P25, and 470 nm for Ag@CuO1:1/P25 and Ag@CuO3:1/P25 (see Fig. 6 and Fig. S5). The absorption in the IR is very broad with a maximum at ca. 800 nm

1  
2  
3 for the two samples rich in Cu (Ag@CuO1:3/P25 and Ag@CuO1:1/P25), while the  
4  
5 sample Ag@CuO3:1/P25 shows no maximum absorption in this region. Ag NPs are  
6  
7 known to exhibit a LSPR with a maximum at around 410 nm in water. It is well  
8  
9 know that position of LSPR depends on the environment and the support.<sup>44</sup>  
10  
11 Therefore, red-shift of LSPR is usually observed as a result of the coupling between  
12  
13 the metal nanoparticles and TiO<sub>2</sub> support having a high reflective index (the  
14  
15 absorption coefficient and refractive index for anatase at a wavelength of 380 nm are  
16  
17 90 cm<sup>-1</sup> and 2.19, respectively), as already reported for Au/TiO<sub>2</sub>, Ag/TiO<sub>2</sub> and Au-  
18  
19 Cu/TiO<sub>2</sub>.<sup>1,6,7</sup> The addition of CuO to TiO<sub>2</sub>-P25 extends clearly the absorption to  
20  
21 visible light. The absorption band in the near IR is observed in the case of Cu  
22  
23 loading, and this is attributed to  $2E_g \rightarrow 2T_{2g}$  inter-band transitions in the Cu<sup>II</sup>  
24  
25 clusters deposited on different phases and sites of TiO<sub>2</sub> and with strong interaction  
26  
27 with the support.<sup>38</sup>  
28  
29  
30  
31  
32  
33

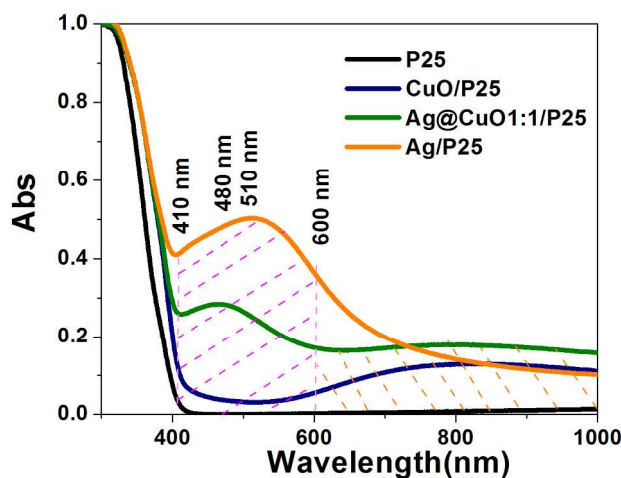


**Figure 6.** UV-Vis diffuse reflectance spectra of the pure TiO<sub>2</sub>-P25 and the modified TiO<sub>2</sub>-P25 with Ag, CuO, and Ag@CuO1:1 showing the regions of the plasmon band of Ag and the absorption band of CuO.

1  
2  
3  
4  
5 The electronic properties of the samples were studied by TRMC technique at  
6  
7 different wavelengths, considering both UV and visible regions. The excitation  
8  
9 wavelengths were 355, 400, 450, 470, 480, 550, 600 and 650 nm and the  
10  
11 corresponding graphs are shown in Fig. 7 and Fig. S6. The surface modification with  
12  
13 Ag and/or CuO NPs shows a strong influence on the charge-carrier dynamics in  
14  
15 TiO<sub>2</sub>-P25.  
16  
17

18  
19 TRMC signals show that, under UV excitation at 355 nm (Fig. 7a), all the  
20  
21 photocatalysts are activated, *i.e.*, free electrons are induced in the CB of TiO<sub>2</sub>-P25,  
22  
23 as shown by the sharp increase of TRMC signal, reaching  $I_{max}$  values. However, the  
24  
25 decay of the signals is faster for the modified samples. The TRMC signals are  
26  
27 mainly related to the electrons having higher mobility than holes. The decrease of  
28  
29 the TRMC signals after modification is probably caused by efficient electron  
30  
31 scavenging by Ag deposits on TiO<sub>2</sub>-P25, resulting in decrease in the recombination  
32  
33 of charge-carriers ( $e^-/h^+$ ). Silver nanoparticles scavenge electrons, but these electrons  
34  
35 can react with oxygen leading to O<sub>2</sub><sup>-</sup> radicals. It has to be noted that oxygen presents  
36  
37 the trend to adsorb on silver, and this will help the formation of superoxide radicals.  
38  
39 At the same time, and because of better separation of charge-carriers, more holes and  
40  
41 OH<sup>·</sup> radicals are generated. It should be pointed that faster decay is observed for  
42  
43 TiO<sub>2</sub>-P25 co-modified with Ag NPs and CuO clusters, and this acceleration  
44  
45 increases with the amount of CuO (Fig. 7a. and Fig. S6a). The photogenerated  
46  
47 electrons can be trapped by Cu<sup>II</sup> (due to the unfilled 3d shell,  $t_{2g}^6 e_g^3$  configuration),  
48  
49 on the surface of TiO<sub>2</sub>-P25, decreasing the recombination process.<sup>45</sup> The TRMC  
50  
51  
52  
53  
54  
55  
56  
57  
58  
59  
60

1  
2  
3 measurements show that Ag@CuO nanoparticles (Ag@CuO(1:3) and Ag@CuO  
4 (1:1)) are very efficient in electron scavenging (see Fig. 7 and Fig. S6a), due to the  
5 synergic effect between Ag and CuO. This acceleration of the signal decay, with  
6  
7  
8 synergic effect between Ag and CuO. This acceleration of the signal decay, with  
9  
10 metal exhibiting capacitive properties, has also been observed for the modification of  
11  
12 TiO<sub>2</sub> with Ag clusters and NPs, Au NPs and Au-Cu NPs.<sup>6,7,15</sup> This observation is  
13  
14 different from our previous results performed with Pt and Pd modified TiO<sub>2</sub>, where a  
15  
16 slowdown of the overall decay was observed.<sup>4,5,46</sup> Indeed, with metals such as Pt and  
17  
18 Pd, the experimental data agree with the model of a simple Schottky-type barrier  
19  
20 between TiO<sub>2</sub> and metal. An increase in the lifetime of the electrons is observed,  
21  
22 due, as expected, to a better separation of charge-carriers caused by the barrier.<sup>46</sup>  
23  
24  
25

26  
27 Nonetheless, an important change is observed in the TRMC signals when the  
28  
29 samples were irradiated at 400 nm (Fig. S6b), *i.e.*, at the transition between the UV  
30  
31 and the visible regions. For P25 and Ag/P25, the  $I_{max}$  values are lower than those  
32  
33 obtained under 355 nm as expected, since the irradiation energy is lower than the  
34  
35 band-gap of anatase, and thus only the rutile phase, being in the minority, can be  
36  
37 activated. However, the samples containing copper reach a higher  $I_{max}$  value, which  
38  
39 represents a higher amount of free electrons in the CB of TiO<sub>2</sub>-P25. This is  
40  
41 consistent with the shift of the band-gap toward the visible region observed by DRS  
42  
43 for these samples compared to bare TiO<sub>2</sub>-P25.  
44  
45  
46

47  
48 Under excitation in the visible region, there is no light absorption by pure TiO<sub>2</sub>-  
49  
50 P25 because of its large band-gap. Under excitation with wavelengths of 450 and  
51  
52 470 (see Fig. 7), TRMC signals are obtained with the samples modified with CuO  
53  
54 due to its narrow band-gap, attesting the generation of free electrons in the  
55  
56 conduction bands of TiO<sub>2</sub>-P25 (see also Figs. S6 e-h). The highest  $I_{max}$ , for all  
57  
58  
59  
60

1  
2  
3 irradiation ranges is obtained for TiO<sub>2</sub>-P25 modified with CuO (CuO/P25). This  
4 suggests that a large amount of excess electrons are injected in the CB of TiO<sub>2</sub>-P25  
5 after excitation of the metal oxide clusters. Thus, under visible light, copper oxide is  
6 excited, and then electrons from its CB are transferred to the CB of the TiO<sub>2</sub>-P25.  
7  
8 This excitation of CuO induces also the same large amount of holes located on these  
9 clusters. However, the decay of the TRMC signals is very fast in the case of  
10 CuO/TiO<sub>2</sub> (Fig. 7b-c). This fast decay is probably due to fast recombination of the  
11 electrons injected from CuO in the conduction band of TiO<sub>2</sub> with excess holes  
12 located on the numerous CuO clusters. However, for the Ag@CuO co-modified  
13 samples, it should be reminded that silver-based NPs are still working as electron  
14 traps decreasing the TRMC signal with the Ag loading. In this case, the electron  
15 coming from excited CuO are not injected in the conduction band of TiO<sub>2</sub>, but they  
16 are trapped by Ag NPs. These electrons probably recombine very fast with the holes  
17 located on CuO because of the large concentration of CuO on AgNPs. It must be  
18 pointed out that electron transfer from silver NPs could not be excluded since TRMC  
19 operates at longer times ( $\mu$ s) than plasmonic excitation, *e.g.*, 240 fs was reported for  
20 electron transfer from 10-nm size gold to titania.<sup>47</sup> At longer wavelengths (600 and  
21 650 nm) (see *Supplementary Information* Fig. S6) only small signals for the samples  
22 with larger amount of copper, *i.e.*, Ag@CuO1:3/P25 and CuO/P25 were detected.  
23  
24  
25  
26  
27  
28  
29  
30  
31  
32  
33  
34  
35  
36  
37  
38  
39  
40  
41  
42  
43  
44  
45  
46  
47  
48  
49  
50  
51  
52  
53  
54  
55  
56  
57  
58  
59  
60

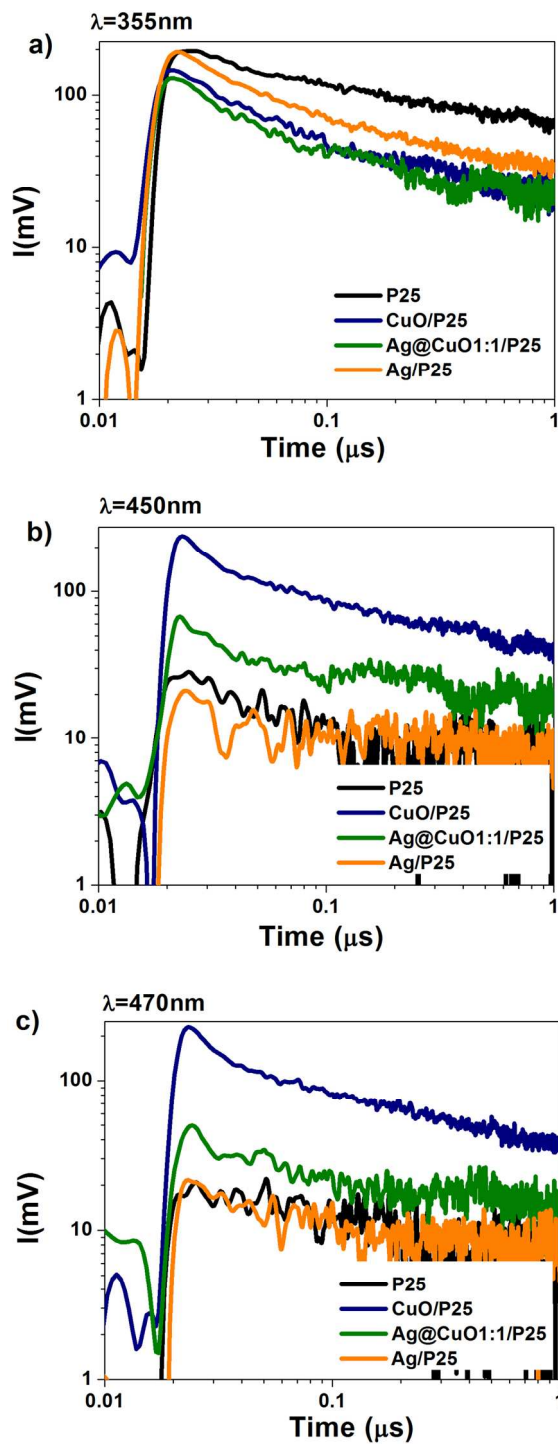


**Figure 7.** TRMC signals obtained after excitation at 355, 450 and 470 nm of TiO<sub>2</sub>-P25, bare and modified with Ag, Ag@CuO1:1 and CuO. The laser energy of these wavelengths were 1.7, 6.7 and 6.2 mJ cm<sup>-2</sup>, respectively.

1  
2  
3 These results show that under visible light excitation, electrons are promoted from  
4 CuO NPs to the CB of TiO<sub>2</sub>-P25. Also, it is worth noting that copper oxide clusters  
5 are able to activate the TiO<sub>2</sub>-P25 photocatalyst in a wider range of wavelengths  
6 under visible light irradiation, compared to the activation with the presence of silver.  
7  
8  
9  
10  
11  
12  
13

### 14 **3.3. Photocatalytic Tests**

15  
16  
17 The photocatalytic activity of the modified TiO<sub>2</sub>-P25 samples was evaluated for  
18 the degradation of phenol and acetic acid under UV and visible light.  
19  
20  
21

22 The curves for phenol degradation are shown in Fig. 8. Surface modification of  
23 TiO<sub>2</sub>-P25 with Ag NPs and CuO clusters does not influence markedly the  
24 photocatalytic activity of TiO<sub>2</sub>-P25 under UV light. However, an enhancement of the  
25 photocatalytic activity is observed for samples modified with Ag@CuO clusters.  
26 Under UV irradiation, (Fig. 8a) the Ag-CuO modified titania and Ag@CuO1:1/P25,  
27 (see also the systems Ag@CuO3:1/P25, Ag@CuO1:3/P25 in Fig. S7-1a) achieve the  
28 complete degradation of phenol after 15 minutes. The kinetic data can be fitted with  
29 a pseudo-first order reaction and the estimated reaction rates are shown in Table 3  
30 and S2. Under UV excitation, the oxidation is due to HO· and O<sub>2</sub><sup>·-</sup> radicals, but  
31 under visible light the oxidation is mainly due to O<sub>2</sub><sup>·-</sup> radicals. We considered zero  
32 order for visible light and pseudo first order for UV light excitation which fits better  
33 the curves, but it does not have a physical meaning as the mechanism is much more  
34 complex.  
35  
36  
37  
38  
39  
40  
41  
42  
43  
44  
45  
46  
47  
48  
49  
50  
51  
52  
53

54  
55 The highest photocatalytic activity is obtained with the sample Ag@CuO1:1/P25  
56 with a reaction rate of around  $3.4 \times 10^{-3} \text{ s}^{-1}$ , which is approximately 1.2 times higher  
57  
58  
59  
60

1  
2  
3 than that of bare TiO<sub>2</sub>-P25 ( $2.5 \times 10^{-3} \text{ s}^{-1}$ ). This increase in the photocatalytic activity  
4  
5 is attributable to the reduction of the recombination process of the charge-carriers  
6  
7 due to the electron scavenging by Ag NPs and to the reduction of Cu<sup>II</sup> into Cu<sup>I</sup>.<sup>45</sup>  
8  
9 Foster *et al.* found that the oxidation of Cu<sup>I</sup> into Cu<sup>II</sup> by O<sub>2</sub> decreased the electron-  
10  
11 hole recombination.<sup>48</sup> These photocatalytic results can be related to the TRMC  
12  
13 signals: TRMC data ( $\lambda_{\text{ex}}=355 \text{ nm}$ ) indicate electron sinking by co-modification with  
14  
15 Ag and CuO clusters (lower  $I_{\text{max}}$  and faster decay, Fig. 7a) beneficial for the  
16  
17 photocatalytic activity.  
18  
19  
20  
21

22 However, surface modification with Ag and/or CuO NPs, significantly increases  
23  
24 the photoactivity of TiO<sub>2</sub>-P25 under visible irradiation.  
25  
26

27 Under visible light, the photoactivity of the pure TiO<sub>2</sub>-P25 is usually very low  
28  
29 because the illumination energy is lower than the band-gap energy. Modification of  
30  
31 titania results in visible photocatalytic activity, as shown in Fig. 8b and Fig. S7-1b  
32  
33 for phenol degradation. The modification with CuO leads to a slightly higher  
34  
35 enhancement in the photocatalytic properties compared to the modification with Ag  
36  
37 or Ag@CuO. 25% and 17% phenol degradation are reached after 4-hour irradiation  
38  
39 of CuO/P25 and Ag/P25, respectively. Surface modification with silver and copper  
40  
41 oxide nanoparticles changes the absorption properties of the photocatalysts,  
42  
43 particularly as an enhancement of the absorption in the visible range creating an  
44  
45 activity under visible light.  
46  
47  
48  
49

50 The CuO/P25 sample exhibits the highest photocatalytic activity for phenol  
51  
52 degradation under visible light. This photocatalytic activity can be related to the  
53  
54 TRMC signals as previously discussed: The CuO/P25 sample showed the highest  
55  
56  
57  
58  
59  
60

$I_{max}$  value in a wide range of excitation wavelengths within the visible range (Figs. 7b and 7c), which represents more electrons in the CB of the semiconductor  $\text{TiO}_2$ -P25. The corresponding kinetics data following a zero order for the degradation of phenol under visible light are shown in Table 3 and S2. The highest values of the reaction rates are obtained with Ag/P25 and CuO/P25. It has to be noted that the CuO/P25 sample shows a reaction rate seven times higher than bare  $\text{TiO}_2$ -P25, thus demonstrating the enhancement of the photoactivity of  $\text{TiO}_2$ -P25 with its surface modification with CuO.

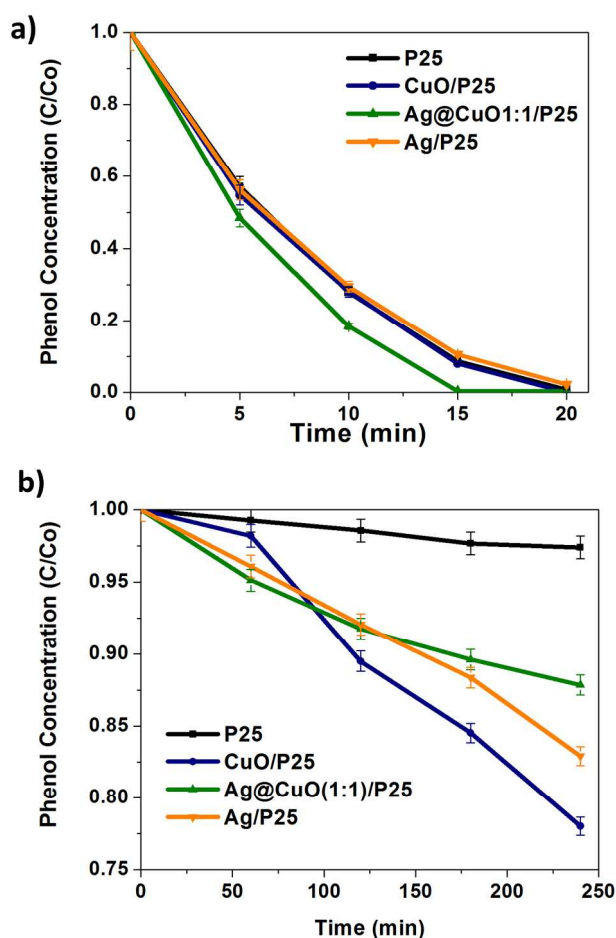


**Figure 8.** Degradation curves of phenol under a) UV and b) visible light ( $\lambda > 450$  nm) for bare and modified (with, Ag, Ag@CuO1:1 and CuO)  $\text{TiO}_2$ -P25.

**Table 3.** Photocatalytic reaction rates for phenol degradation with Ag/P25, CuO/P25 and Ag@CuO1:1/P25 under UV irradiation (pseudo-first order reaction) and visible light (zero order reaction). The relative uncertainty for UV light is 5% and for visible light is 3%.

Sample	UV light	Visible light
	( $\times 10^{-3} \text{ s}^{-1}$ )	( $\times 10^{-4} \text{ M s}^{-1}$ )
P25	2.5	0.9
CuO/P25	2.6	7.5
Ag@CuO1:1/P25	3.4	3.6
Ag/P25	2.3	5.3

The modified TiO<sub>2</sub>-P25 samples were also evaluated for the photocatalytic evolution of CO<sub>2</sub> as a result of the decomposition of acetic acid under monochromatic irradiation. Exemplary data for two different irradiation regions, *i.e.*, UV at  $\lambda=350$  nm, and visible light at  $\lambda=470$  nm, are shown in Fig. 9, Fig. S7-2a and Fig. S7-2b.

Fig. 9 shows that the modified TiO<sub>2</sub>-P25 samples, are in general more active in the generation of CO<sub>2</sub> compared to bare TiO<sub>2</sub>-P25, especially under visible light. Under UV irradiation, at 350 nm (Fig. 9a), the modified titania are more active than bare TiO<sub>2</sub>-P25. TRMC signals at 355 nm show that CuO-based nanoparticles on TiO<sub>2</sub>-P25 are efficient in electron scavenging (Fig. 7a). This higher photocatalytic activity (higher generation of CO<sub>2</sub>) at 350 nm for TiO<sub>2</sub>-P25 modified with CuO-based nanoparticles (Ag, Ag@CuO1:3, Ag@CuO1:1 and CuO) can be caused by better charge-carrier separation, with exception of Ag@CuO3:1/P25 sample (see Fig. S7-2a).

Under visible light at 470 nm irradiation (Fig. 9b and Fig. S7-2b), surface modified TiO<sub>2</sub>-P25 with Ag and CuO clusters are more active in the production of CO<sub>2</sub> compared to bare TiO<sub>2</sub>-P25. Surface modification with CuO nanoclusters induces a higher increase in the photocatalytic activity under visible light compared to the modification with plasmonic Ag and Ag@CuO nanoparticles. The highest production of CO<sub>2</sub> is again obtained with CuO/P25. Indeed, it has to be noted that CuO/P25 presents a higher TRMC signal at 470 nm compared to Ag@CuO/P25, and this indicates that more electrons are generated in the CB of CuO-modified TiO<sub>2</sub>-P25.

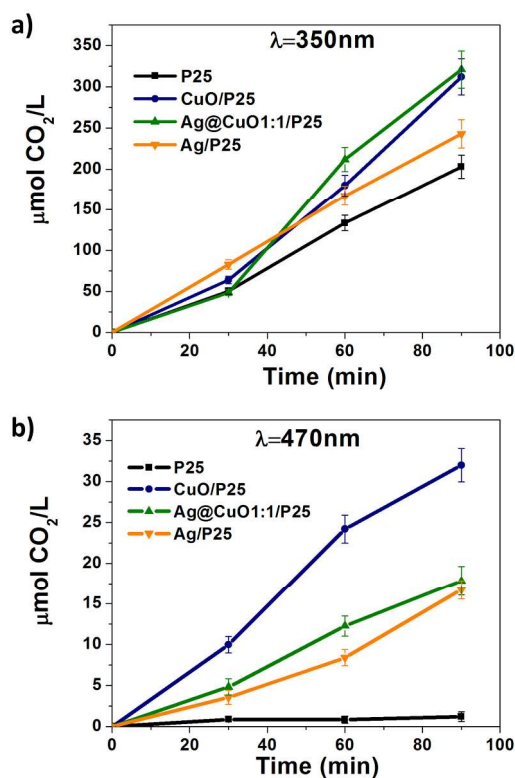


**Figure 9.** Photocatalytic evolution of CO<sub>2</sub> resulting from the decomposition of acetic acid under irradiation with a) 350 nm, and b) 470 nm for the pure system TiO<sub>2</sub>-P25 and modified systems with, Ag, Ag@CuO1:1 and CuO.

Based on acetic acid decomposition at various monochromatic irradiations, the AS of the synthesized samples were obtained, and the results are shown in Fig. 10 and the S8g. The samples containing mainly CuO/P25 exhibit higher activity than bare TiO<sub>2</sub>-P25 under UV irradiation. In the visible range, the modified TiO<sub>2</sub>-P25 with Ag and CuO shows higher apparent quantum efficiency in the range between 410–500 nm, which can be related to the LSPR of silver and to the injection of electrons from CuO in the CB of TiO<sub>2</sub>-P25.

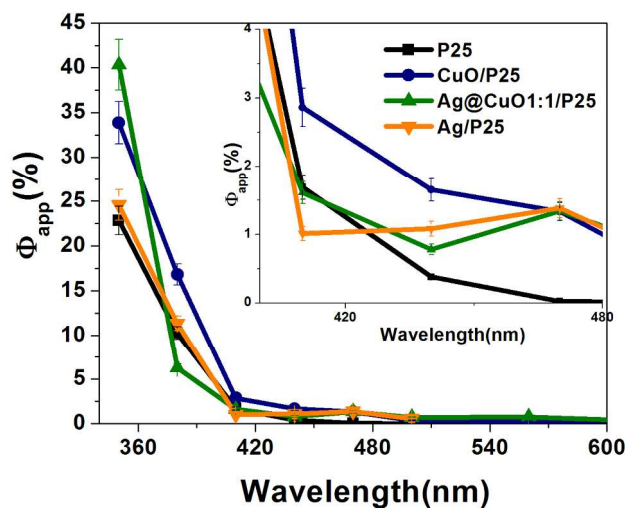


**Figure 10.** Action spectra for the acetic acid decomposition on bare and modified TiO<sub>2</sub>-P25 (with Ag, CuO and Ag@CuO1:1).

It has to be noted that, under visible light, for both phenol degradation and CO<sub>2</sub> generation, the modification with CuO induces the highest photocatalytic activity. These results are shown in Fig. 8b and Fig. 9b. In the case of CuO/P25, CuO is in direct contact with TiO<sub>2</sub>, and a high amount of electrons are directly injected from CuO into the CB of TiO<sub>2</sub>-P25 as is shown by the TRMC signals under excitation with the visible light. However, in the case of TiO<sub>2</sub>-P25 modified with Ag@CuO,

1  
2  
3 the CuO shell is deposited on Ag nanoparticles. Under visible light excitation, the  
4  
5 electrons cannot be directly injected from CuO into the CB of TiO<sub>2</sub>-P25, due to the  
6  
7 interaction of the Ag<sub>core</sub>@CuO<sub>shell</sub> structure. This is consistent with the TRMC  
8  
9 signals under visible excitation, which are lower for Ag@CuO/P25 than for  
10  
11 CuO/P25 (Fig. 7b-c), affecting the photoactivity as is shown in most of the tested  
12  
13 reactions, where the activity of Ag@CuO/P25 samples is lower than that of Ag/P25  
14  
15 and CuO/P25.  
16  
17  
18  
19

20 The AS were compared to the absorption spectra obtained by DRS (Fig. S8) and  
21 they indicate that the photoreaction is carried out by a photocatalytic mechanism.<sup>49</sup>  
22  
23 Action spectrum correlates well with absorption spectrum for bare titania, reaching  
24  
25 quantum yield of 22.8%, 10.2% and 1.7% for irradiation with 350, 380 and 410 nm,  
26  
27 respectively. However, for the modified samples, only a part of the absorption  
28  
29 spectra (below 480 nm) correlates with their photocatalytic activity, reaching a  
30  
31 maximum at 470 nm, which confirms that LSPR of Ag NPs and the narrow band-  
32  
33 gap of CuO are responsible for the photocatalytic activity under visible light  
34  
35 irradiation.  
36  
37  
38  
39

40 CuO/P25 and Ag@CuO/P25 exhibit no photocatalytic activity at  $\lambda > 500$  nm  
41  
42 (negligible quantum efficiency) but present small TRMC signals: We hypothesized  
43  
44 that these generated electrons with lower energy are mobile but inactive for  
45  
46 degradation of organic compounds or these electrons are reactive but with lower  
47  
48 quantum yield.  
49  
50  
51

52 It is important to mention that the DRS of dried Ag-modified samples differ  
53  
54 from suspended ones,<sup>15,50</sup> showing a red-shift due to enhanced scattering, which is  
55  
56 highly dependent on particle size and shape,<sup>42</sup> contrasting with Au/TiO<sub>2</sub> systems,  
57  
58  
59  
60

1  
2  
3 that shows almost the same DRS.<sup>9</sup>  
4

5 These combined results by TRMC and AS sheds light on the photocatalytic  
6 mechanism: Under UV light, the Ag nanoparticles and CuO clusters work as  
7 electron pools, retarding the recombination process as it is supported by the TRMC  
8 results. This scavenging phenomenon helps to increase the photoreactions due to the  
9 formation of the Schottky junction when Ag and CuO are in contact with the  
10 semiconductor TiO<sub>2</sub>-P25. It is known that coupling of TiO<sub>2</sub> with other  
11 semiconductors of different redox energy levels can lead to more efficient charge-  
12 carrier separation process, *i.e.*, an increase in the lifetime of the charge-carriers and  
13 an enhancement of the interfacial charge-transfer efficiency to adsorbed  
14 substrate.<sup>51,52</sup> It is proposed that electrons trapped by CuO would react with adsorbed  
15 oxygen or air retarding (or inhibiting) the electron-hole recombination.<sup>45</sup> TRMC  
16 signals show that Ag@CuO nanoparticles are more efficient in electron scavenging  
17 compared to Ag NPs and CuO clusters, and this leads to higher photocatalytic  
18 activity under UV light. Under visible light excitation, TRMC signals and AS show  
19 that Ag NPs, due to their surface plasmon resonance and CuO due to its narrow  
20 band-gap (1.7 eV)<sup>52</sup> induce an activity in the visible. It has to be noted that this  
21 energy band-gap value increases with the size of CuO, *e.g.*, Ge *et al.* reported that  
22 for CuO nanoclusters, the band-gap decreases from 2.6 eV to 1.4 eV when the size  
23 increases from 1.1 nm to 2 nm.<sup>53</sup> The CuO clusters are excited under visible light  
24 injecting electrons in the CB of TiO<sub>2</sub>-P25. In case of CuO/P25, more electrons are  
25 injected compared to the other modified samples and this corresponds to higher  
26 photocatalytic activity under visible light. However, the photocatalytic activity under  
27 visible light of TiO<sub>2</sub>-P25 co-modified Ag@CuO clusters is lower than that of  
28  
29  
30  
31  
32  
33  
34  
35  
36  
37  
38  
39  
40  
41  
42  
43  
44  
45  
46  
47  
48  
49  
50  
51  
52  
53  
54  
55  
56  
57  
58  
59  
60

1  
2  
3 CuO/P25 and Ag/P25. This behavior is probably due to the electron scavenging by  
4  
5 Ag, instead of transferring the electrons to the CB of titania.  
6  
7

8 All above discussed results allow to propose photoinduced mechanisms for TiO<sub>2</sub>-  
9 P25 modified with CuO and Ag@CuO nanoparticles under UV and visible light  
10 irradiation, and they are shown in Fig. 11: Under UV irradiation (Fig. 11a), the  
11 number of charge-carriers decreases due to the relaxation of CB photogenerated  
12 electrons on TiO<sub>2</sub>-P25 to the valence band (VB) of CuO, acting in this system as  
13 electron traps. The photocatalytic activity is similar to TiO<sub>2</sub>-P25 for phenol  
14 degradation, but is higher at 350 nm for acetic acid degradation. (Fig. 8a, and Fig.  
15 9a), b). Under visible irradiation (Fig. 11b), due to the position and the value of the  
16 energy band-gap of CuO, visible light photo-generates electrons from CuO, and  
17 these electrons are injected into the CB of TiO<sub>2</sub>-P25, as it can be observed in TMRC  
18 signals in Fig. 7b)-c) at 450 nm and 470 nm. The photoactivity is always higher than  
19 TiO<sub>2</sub>-P25 for all the modified samples (Fig. 8b, and Fig.9b). For, Ag@CuO/P25, in  
20 Fig. 11.a) under UV irradiation, the Ag@CuO NPs scavenge electrons (as shown by  
21 the TRMC signal at 355 nm, Fig. 7a), which induces an increase in the photoactivity  
22 (see Fig. 8, phenol degradation), due to the fact that Ag NPs work as electron traps  
23 of both TiO<sub>2</sub>-P25 and CuO semiconductors. When the systems are irradiated under  
24 visible light, (Fig. 11b) Ag NPs still work as electron traps, trapping the electrons  
25 photogenerated by CuO avoiding a part of injection to the CB of TiO<sub>2</sub>-P25,  
26 decreasing the TRMC signals, and thus decreasing the photoactivity.  
27  
28  
29  
30  
31  
32  
33  
34  
35  
36  
37  
38  
39  
40  
41  
42  
43  
44  
45  
46  
47  
48  
49  
50  
51  
52  
53  
54  
55  
56  
57  
58  
59  
60

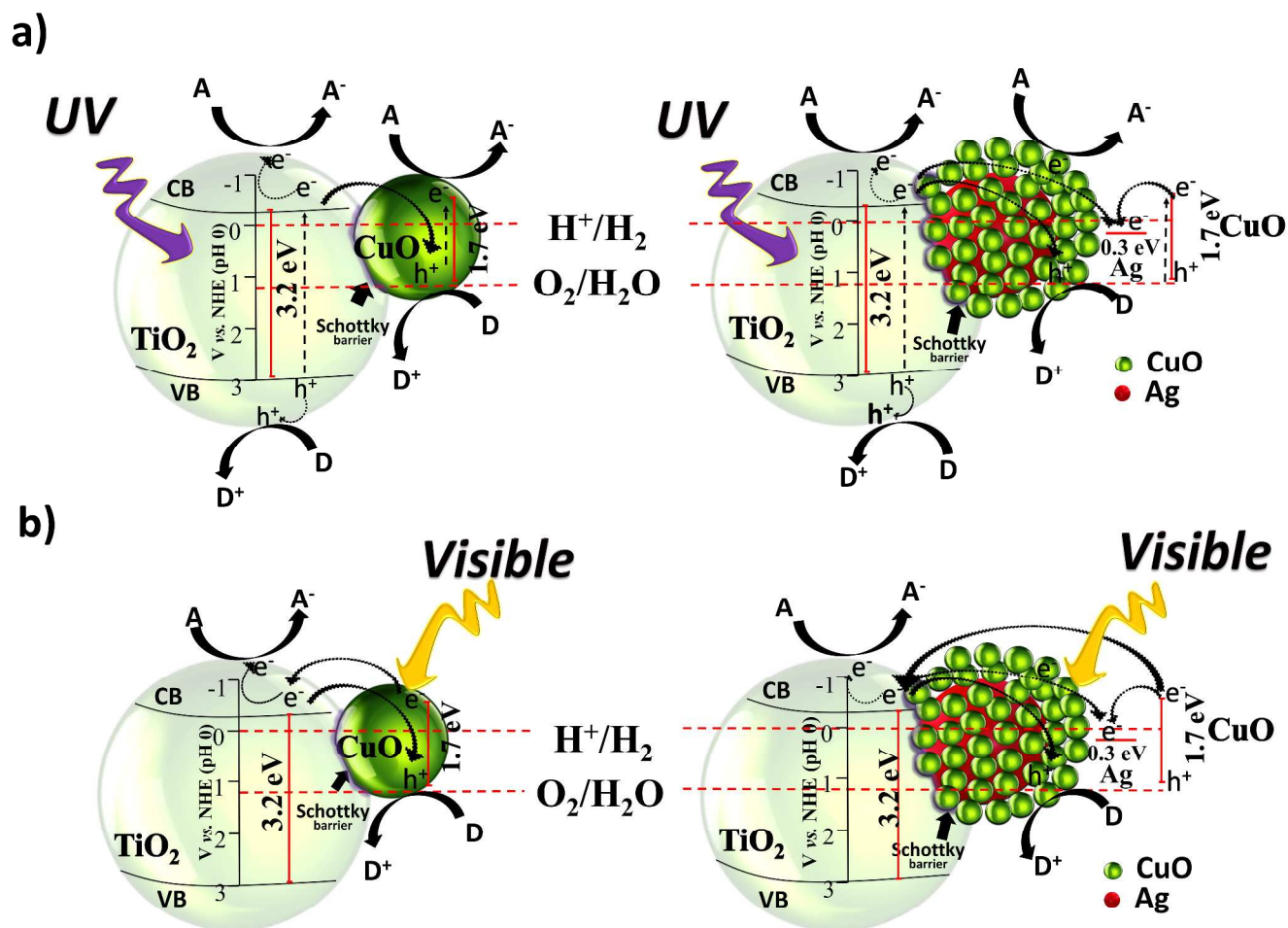


**Figure 11.** Proposed photocatalytic mechanisms of TiO<sub>2</sub>-P25 modified with CuO and Ag@CuO; a) under UV and b) under visible irradiation.

## Conclusions

CuO clusters, Ag and Ag@CuO NPs were synthesized by radiolysis on the surface of TiO<sub>2</sub>-P25. HAADF-STEM, XPS and XAS characterization have shown that, in case of co-modification with silver and copper, core-shell nanoparticles composed of silver cores decorated with small CuO clusters were obtained on TiO<sub>2</sub>-

1  
2  
3 P25. Surface modification with Ag, Ag@CuO and CuO nanoparticles induces an  
4  
5 enhancement in the photocatalytic activity of TiO<sub>2</sub>-P25, under both UV and visible  
6  
7 light. Catalytic tests for phenol and acetic acid degradation show that co-  
8  
9 modification of TiO<sub>2</sub>-P25 with CuO and Ag nanoparticles induces a higher  
10  
11 photocatalytic activity under UV light compared to single modification with only Ag  
12  
13 or CuO clusters, while the contrary is obtained under visible light. Under visible  
14  
15 light, CuO-modified titania exhibits higher activity than plasmonic Ag/P25 and  
16  
17 Ag@CuO/P25. TRMC results show that under excitation with UV light, metal Ag  
18  
19 NPs, Ag@CuO and CuO clusters act as electron traps decreasing the recombination  
20  
21 process, and thus, they present a highly increment in the apparent quantum yield.  
22  
23 Under visible excitation, the Ag nanoparticles absorb incident photons due to the  
24  
25 LSPR and inject electrons into the CB of TiO<sub>2</sub>-P25, as is shown by TRMC  
26  
27 measurements. CuO are excited in the visible range because of their band-gap, and  
28  
29 the electrons are driven from the CB of CuO to the CB of TiO<sub>2</sub>-P25.  
30  
31  
32  
33  
34  
35

36 In general, the photocatalytic activity of the samples containing CuO is higher,  
37  
38 which induces a photocatalytic activity in a wider spectral range compared to that  
39  
40 obtained with modification with silver. AS prove that decomposition of acetic acid is  
41  
42 driven by photocatalytic reaction, and Ag and CuO modification results in high  
43  
44 enhancement of quantum yield under UV and visible light irradiation. However,  
45  
46 only a shorter part of visible absorption (< 500 nm) is responsible for photocatalytic  
47  
48 activity. For the oxidation reactions tested in this study under visible light  
49  
50 irradiation, surface co-modification of TiO<sub>2</sub>-P25 with Ag@CuO clusters leads to  
51  
52 samples with lower activity compared to Ag/P25 and CuO/P25.  
53  
54  
55  
56  
57  
58  
59  
60

1  
2  
3 The antibacterial and antifungal properties of titania modified with copper and  
4 silver are under investigation.  
5  
6  
7  
8  
9

### †Supporting Information

10  
11  
12 Additional energy dispersive X-ray spectroscopy line scans and STEM-HAADF images of  
13 Ag and Cu-modified TiO<sub>2</sub>, additional TRMC signals, XPS analysis and the photocatalytic  
14 tests for the samples with different ratios Ag/CuO are presented in the Supporting  
15 Information file. This material is available free of charge via the Internet at  
16 <http://www.pubs.acs.org/>.  
17  
18  
19  
20  
21  
22  
23  
24  
25  
26

### Acknowledgements

27  
28  
29 The authors thank Arnaud Etcheberry (ILV, Université Versailles Saint-Quentin  
30 en Yvelines) for helpful discussions and Emiliano Fonda (SOLEIL, Saint-Aubin) for  
31 providing the beamtime at the SAMBA beamline. Financial support from the CNRS,  
32 ECOS-Nord M11-P02 project (CNRS-CONACYT bilateral project), the  
33 CONCERT-Japan Joint Call on Efficient Energy Storage (European Commission),  
34 the COST Nanoalloys and CONACYT (Mexico grant numbers 106437, 216315 and  
35 356872) are highly acknowledged. M.G.M.M. acknowledges Campus France for the  
36 *Eiffel Excellence* Scholarship. The authors acknowledge also C’Nano Ile de France  
37 for the financial support for *the gamma source and* for TRMC setup. The RTRA  
38 Triangle de la Physique and the ANR project PhotoNorm are also acknowledged for  
39 the TRMC setup.  
40  
41  
42  
43  
44  
45  
46  
47  
48  
49  
50  
51  
52  
53  
54  
55  
56  
57  
58  
59  
60

## References

- (1) Linic, S.; Christopher, P.; Ingram, D. B. Plasmonic-Metal Nanostructures for Efficient Conversion of Solar to Chemical Energy. *Nat. Mater.* **2011**, *10*, 911–921.
- (2) Zhang, X.; Chen, Y. L.; Liu, R.-S.; Tsai, D. P. Plasmonic Photocatalysis. *Rep. Prog. Phys.* **2013**, *76*, 046401.
- (3) Banerjee, S.; Pillai, S. C.; Falaras, P.; O’Shea, K. E.; Byrne, J. A.; Dionysiou, D. D. New Insights into the Mechanism of Visible Light Photocatalysis. *J. Phys. Chem. Lett.* **2014**, *5*, 2543–2554.
- (4) Kowalska, E.; Remita, H.; Colbeau-Justin, C.; Hupka, J.; Belloni, J. Modification of Titanium Dioxide with Platinum Ions and Clusters: Application in Photocatalysis. *J. Phys. Chem. C* **2008**, *112*, 1124–1131.
- (5) Tahiri Alaoui, O.; Herissan, A.; Le Quoc, C.; Zekri, M. el M.; Sorgues, S.; Remita, H.; Colbeau-Justin, C. Elaboration, Charge-Carrier Lifetimes and Activity of Pd-TiO<sub>2</sub> Photocatalysts Obtained by Gamma Radiolysis. *J. Photochem. Photobiol. Chem.* **2012**, *242*, 34–43.
- (6) Grabowska, E.; Zaleska, A.; Sorgues, S.; Kunst, M.; Etcheberry, A.; Colbeau-Justin, C.; Remita, H. Modification of Titanium(IV) Dioxide with Small Silver Nanoparticles: Application in Photocatalysis. *J. Phys. Chem. C* **2013**, *117*, 1955–1962.
- (7) Hai, Z.; Kolli, N. E.; Uribe, D. B.; Beaunier, P.; José-Yacaman, M.; Vigneron, J.; Etcheberry, A.; Sorgues, S.; Colbeau-Justin, C.; Chen, J.; et al. Modification of TiO<sub>2</sub> by Bimetallic Au–Cu Nanoparticles for Wastewater Treatment. *J. Mater. Chem. A* **2013**, *1*, 10829–10835.

- 1  
2  
3 (8) Hai, Z.; Kolli, N. E.; Chen, J.; Remita, H. Radiolytic Synthesis of Au–Cu Bimetallic  
4 Nanoparticles Supported on TiO<sub>2</sub>: Application in Photocatalysis. *New J. Chem.* **2014**, *38*,  
5 5279–5286.  
6  
7  
8  
9  
10 (9) Kowalska, E.; Mahaney, O. O. P.; Abe, R.; Ohtani, B. Visible-Light-Induced  
11 Photocatalysis through Surface Plasmon Excitation of Gold on Titania Surfaces. *Phys.*  
12 *Chem. Chem. Phys.* **2010**, *12*, 2344–2355.  
13  
14  
15 (10) Shiraishi, Y.; Sakamoto, H.; Sugano, Y.; Ichikawa, S.; Hirai, T. Pt–Cu Bimetallic  
16 Alloy Nanoparticles Supported on Anatase TiO<sub>2</sub>: Highly Active Catalysts for Aerobic  
17 Oxidation Driven by Visible Light. *ACS Nano* **2013**, *7*, 9287–9297.  
18  
19  
20 (11) Qiu, X.; Miyauchi, M.; Yu, H.; Irie, H.; Hashimoto, K. Visible-Light-Driven Cu(II)-  
21 (Sr(1-y)Na(y))(Ti(1-x)Mo(x))O<sub>3</sub> Photocatalysts Based on Conduction Band Control and  
22 Surface Ion Modification. *J. Am. Chem. Soc.* **2010**, *132*, 15259–15267.  
23  
24  
25 (12) Luna, A. L.; Valenzuela, M. A.; Colbeau-Justin, C.; Vázquez, P.; Rodriguez, J. L.;  
26 Avendaño, J. R.; Alfaro, S.; Tirado, S.; Garduño, A.; De la Rosa, J. M. Photocatalytic  
27 Degradation of Gallic Acid over CuO–TiO<sub>2</sub> Composites under UV/Vis LEDs Irradiation.  
28 *Appl. Catal. Gen.* **2015**, DOI:10.1016/j.apcata.2015.10.044.  
29  
30  
31 (13) Zhao, L.; Cui, T.; Li, Y.; Wang, B.; Han, J.; Han, L.; Liu, Z. Efficient Visible Light  
32 Photocatalytic Activity of P–n Junction CuO/TiO<sub>2</sub> Loaded on Natural Zeolite. *RSC Adv.*  
33 **2015**, *5*, 64495–64502.  
34  
35  
36 (14) Zielińska-Jurek, A.; Kowalska, E.; Sobczak, J. W.; Lisowski, W.; Ohtani, B.;  
37 Zaleska, A. Preparation and Characterization of Monometallic (Au) and Bimetallic (Ag/Au)  
38 Modified-Titania Photocatalysts Activated by Visible Light. *Appl. Catal. B Environ.* **2011**,  
39 *101*, 504–514.  
40  
41  
42  
43  
44  
45  
46  
47  
48  
49  
50  
51  
52  
53  
54  
55  
56  
57  
58  
59  
60

- 1  
2  
3 (15) Kowalska, E.; Wei, Z.; Karabiyik, B.; Herissan, A.; Janczarek, M.; Endo, M.;  
4  
5 Markowska-Szczupak, A.; Remita, H.; Ohtani, B. Silver-Modified Titania with Enhanced  
6  
7 Photocatalytic and Antimicrobial Properties under UV and Visible Light Irradiation. *Catal.*  
8  
9 *Today* **2015**, *252*, 136–142.  
10  
11  
12 (16) Irie, H.; Miura, S.; Kamiya, K.; Hashimoto, K. Efficient Visible Light-Sensitive  
13  
14 Photocatalysts: Grafting Cu(II) Ions onto TiO<sub>2</sub> and WO<sub>3</sub> Photocatalysts. *Chem. Phys. Lett.*  
15  
16 **2008**, *457*, 202–205.  
17  
18  
19 (17) Ovcharov, M. L.; Shvalagin, V. V.; Granchak, V. M. Photocatalytic Reduction of  
20  
21 CO<sub>2</sub> on Mesoporous TiO<sub>2</sub> Modified with Ag/Cu Bimetallic Nanostructures. *Theor. Exp.*  
22  
23 *Chem.* **2014**, *50*, 175–180.  
24  
25  
26 (18) Ohtani, B.; Prieto-Mahaney, O. O.; Li, D.; Abe, R. What Is Degussa (Evonik) P25?  
27  
28 Crystalline Composition Analysis, Reconstruction from Isolated Pure Particles and  
29  
30 Photocatalytic Activity Test. *J. Photochem. Photobiol. Chem.* **2010**, *216*, 179–182.  
31  
32  
33 (19) Remita, H.; Remita, S. Metal Clusters and Nanomaterials: Contribution of Radiation  
34  
35 Chemistry. In *Recent Trends in Radiation Chemistry*; World Scientific, 2010; pp 347–383.  
36  
37  
38 (20) Belloni, J.; Mostafavi, M.; Remita, H.; Marignier, J.L.; Delcourt, and M.-O.  
39  
40 Radiation-Induced Synthesis of Mono- and Multi-Metallic Clusters and Nanocolloids. *New*  
41  
42 *J. Chem.* **1998**, *22*, 1239–1255.  
43  
44  
45 (21) Colbeau-Justin, C.; Kunst, M.; Huguenin, D. Structural Influence on Charge-Carrier  
46  
47 Lifetimes in TiO<sub>2</sub> Powders Studied by Microwave Absorption. *J. Mater. Sci.* **2003**, *38*,  
48  
49 2429–2437.  
50  
51  
52 (22) Kouamé, N. A.; Alaoui, O. T.; Herissan, A.; Larios, E.; José-Yacaman, M.;  
53  
54 Etcheberry, A.; Colbeau-Justin, C.; Remita, H. Visible Light-Induced Photocatalytic  
55  
56  
57  
58  
59  
60

1  
2  
3 Activity of Modified titanium(IV) Oxide with Zero-Valent Bismuth Clusters. *New J. Chem.*  
4  
5 **2015**, *39*, 2316–2322.

6  
7  
8 (23) Martin, S. T.; Herrmann, H.; Choi, W.; Hoffmann, M. R. Time-Resolved  
9  
10 Microwave Conductivity. Part 1. TiO<sub>2</sub> Photoreactivity and Size Quantization. *J. Chem. Soc.*  
11  
12 *Faraday Trans.* **1994**, *90*, 3315.

13  
14  
15 (24) Khatouri, J.; Mostafavi, M.; Amblard, J.; Belloni, J. Radiation-Induced Copper  
16  
17 Aggregates and Oligomers. *Chem. Phys. Lett.* **1992**, *191*, 351–356.

18  
19  
20 (25) Hansen, M.; Elliott, R. P.; Shunk, F. A. *Constitution of binary alloys.*, 15a ed.;  
21  
22 McGraw-Hill: New York, 1958.

23  
24  
25 (26) Lequien, F.; Creuze, J.; Berthier, F.; Braems, I.; Legrand, B. Superficial  
26  
27 Segregation, Wetting, and Dynamical Equilibrium in Bimetallic Clusters: A Monte Carlo  
28  
29 Study. *Phys. Rev. B* **2008**, *78*, 075414.

30  
31  
32 (27) Moreno, V.; Creuze, J.; Berthier, F.; Mottet, C.; Tréglia, G.; Legrand, B. Site  
33  
34 Segregation in Size-Mismatched Nanoalloys: Application to Cu–Ag. *Surf. Sci.* **2006**, *600*,  
35  
36 5011–5020.

37  
38  
39 (28) Lequien, F.; Creuze, J.; Berthier, F.; Legrand, B. Dynamical Equilibrium in  
40  
41 Nanoalloys. *Faraday Discuss.* **2008**, *138*, 105–117;

42  
43  
44 (29) Guisbiers, G.; Mendoza-Cruz, R.; Bazán-Díaz, L.; Velázquez-Salazar, J. J.;  
45  
46 Mendoza-Perez, R.; Robledo-Torres, J. A.; Rodriguez-Lopez, J.L.; Montejano-Carrizales, J.  
47  
48 M.; Whetten, R. L.; José-Yacamán, M. Electrum, the Gold–Silver Alloy, from the Bulk  
49  
50 Scale to the Nanoscale: Synthesis, Properties, and Segregation Rules. *ACS Nano.* **2015**,  
51  
52 DOI:10.1021/acsnano.5b05755.

- 1  
2  
3 (30) Pellarin, M.; Issa, I.; Langlois, C.; Lebeault, M.-A.; Ramade, J.; Lermé, J.; Broyer,  
4 M.; Cottancin, E. Plasmon Spectroscopy and Chemical Structure of Small Bimetallic Cu(1-  
5 x)Ag<sub>x</sub> Clusters. *J. Phys. Chem. C* **2015**, *119*, 5002–5012.  
6  
7  
8  
9  
10 (31) Verbruggen, S. W.; Keulemans, M.; Filippousi, M.; Flahaut, D.; Van Tendeloo, G.;  
11 Lacombe, S.; Martens, J. A.; Lenaerts, S. Plasmonic Gold–silver Alloy on TiO<sub>2</sub>  
12 Photocatalysts with Tunable Visible Light Activity. *Appl. Catal. B Environ.* **2014**, *156*,  
13 116–121.  
14  
15  
16  
17  
18  
19 (32) Stathatos, E.; Lianos, P.; Falaras, P.; Siokou, A. Photocatalytically Deposited Silver  
20 Nanoparticles on Mesoporous TiO<sub>2</sub> Films. *Langmuir* **2000**, *16*, 2398–2400.  
21  
22  
23  
24 (33) Waterhouse, G. I. N.; Bowmaker, G. A.; Metson, J. B. Oxidation of a  
25 Polycrystalline Silver Foil by Reaction with Ozone. *Appl. Surf. Sci.* **2001**, *183*, 191–204.  
26  
27  
28  
29 (34) Biemann, M.; Schwaller, P.; Ruffieux, P.; Gröning, O.; Schlapbach, L.; Gröning, P.  
30 AgO Investigated by Photoelectron Spectroscopy: Evidence for Mixed Valence. *Phys. Rev.*  
31 *B* **2002**, *65*, 235431.  
32  
33  
34  
35  
36 (35) Han, Y.; Lupitsky, R.; Chou, T.-M.; Stafford, C. M.; Du, H.; Sukhishvili, S. Effect  
37 of Oxidation on Surface-Enhanced Raman Scattering Activity of Silver Nanoparticles: A  
38 Quantitative Correlation. *Anal. Chem.* **2011**, *83*, 5873–5880.  
39  
40  
41  
42  
43 (36) Espinós, J. P.; Morales, J.; Barranco, A.; Caballero, A.; Holgado, J. P.; González-  
44 Elipe, A. R. Interface Effects for Cu, CuO, and Cu<sub>2</sub>O Deposited on SiO<sub>2</sub> and ZrO<sub>2</sub>. XPS  
45 Determination of the Valence State of Copper in Cu/SiO<sub>2</sub> and Cu/ZrO<sub>2</sub> Catalysts. *J. Phys.*  
46 *Chem. B* **2002**, *106*, 6921–6929.  
47  
48  
49  
50  
51  
52 (37) Pauly, N.; Tougaard, S.; Yubero, F. Determination of the Cu 2p Primary Excitation  
53 Spectra for Cu, Cu<sub>2</sub>O and CuO. *Surf. Sci.* **2014**, *620*, 17–22.  
54  
55  
56  
57  
58  
59  
60

- 1  
2  
3 (38) Colón, G.; Maicu, M.; Hidalgo, M. C.; Navío, J. A. Cu-Doped TiO<sub>2</sub> Systems with  
4 Improved Photocatalytic Activity. *Appl. Catal. B Environ.* **2006**, *67*, 41–51.  
5  
6  
7  
8 (39) Peters, S.; Peredkov, S.; Neeb, M.; Eberhardt, W.; Al-Hada, M. Size-Dependent  
9 XPS Spectra of Small Supported Au-Clusters. *Surf. Sci.* **2013**, *608*, 129–134.  
10  
11  
12 (40) Chusuei, C. C.; Brookshier, M. A.; Goodman, D. W. Correlation of Relative X-Ray  
13 Photoelectron Spectroscopy Shake-up Intensity with CuO Particle Size. *Langmuir* **1999**,  
14 *15*, 2806–2808.  
15  
16  
17  
18 (41) Klepka, M. T.; Drzewiecka, A.; Wolska, A.; Ferenc, W. XAS Studies on Cu(II)  
19 Complexes with Derivatives of Phenoxyacetic and Benzoic Acids. *Chem. Phys. Lett.* **2012**,  
20 *553*, 59–63.  
21  
22  
23  
24 (42) Chettibi, S.; Keghouche, N.; Benguedouar, Y.; Bettahar, M. M.; Belloni, J.  
25 Structural and Catalytic Characterization of Radiation-Induced Ni/TiO<sub>2</sub> Nanoparticles.  
26 *Catal. Lett.* **2013**, *143*, 1166–1174.  
27  
28  
29  
30 (43) Chiarello, G. L.; Selli, E.; Forni, L. Photocatalytic Hydrogen Production over Flame  
31 Spray Pyrolysis-Synthesised TiO<sub>2</sub> and Au/TiO<sub>2</sub>. *Appl. Catal. B Environ.* **2008**, *84*, 332–  
32 339.  
33  
34  
35  
36 (44) Mizeikis, V.; Kowalska, E.; Juodkazis, S. Resonant Localization, Enhancement, and  
37 Polarization of Optical Fields in Nano-Scale Interface Regions for Photo-Catalytic  
38 Applications. *J. Nanosci. Nanotechnol.* **2011**, *11*, 2814–2822.  
39  
40  
41  
42 (45) Chiang, K.; Amal, R.; Tran, T. Photocatalytic Degradation of Cyanide Using  
43 Titanium Dioxide Modified with Copper Oxide. *Adv. Environ. Res.* **2002**, *6*, 471–485.  
44  
45  
46  
47 (46) Emilio, C. A.; Litter, M. I.; Kunst, M.; Bouchard, M.; Colbeau-Justin, C. Phenol  
48 Photodegradation on Platinized-TiO<sub>2</sub> Photocatalysts Related to Charge-Carrier Dynamics.  
49 *Langmuir* **2006**, *22*, 3606–3613.  
50  
51  
52  
53  
54  
55  
56  
57  
58  
59  
60

- 1  
2  
3 (47) Furube, A.; Du, L.; Hara, K.; Katoh, R.; Tachiya, M. Ultrafast Plasmon-Induced  
4 Electron Transfer from Gold Nanodots into TiO<sub>2</sub> Nanoparticles. *J. Am. Chem. Soc.* **2007**,  
5 *129*, 14852–14853.  
6  
7  
8  
9  
10 (48) Foster, N. S.; Noble, R. D.; Koval, C. A. Reversible Photoreductive Deposition and  
11 Oxidative Dissolution of Copper Ions in Titanium Dioxide Aqueous Suspensions. *Environ.*  
12 *Sci. Technol.* **1993**, *27*, 350–356.  
13  
14  
15  
16  
17 (49) Nishijima, K.; Ohtani, B.; Yan, X.; Kamai, T.; Chiyoya, T.; Tsubota, T.; Murakami,  
18 N.; Ohno, T. Incident Light Dependence for Photocatalytic Degradation of Acetaldehyde  
19 and Acetic Acid on S-Doped and N-Doped TiO<sub>2</sub> Photocatalysts. *Chem. Phys.* **2007**, *339*,  
20 *64–72*.  
21  
22  
23  
24  
25  
26  
27 (50) Kowalska, E.; Janczarek, M.; Rosa, L.; Juodkazis, S.; Ohtani, B. Mono- and Bi-  
28 Metallic Plasmonic Photocatalysts for Degradation of Organic Compounds under UV and  
29 Visible Light Irradiation. *Catal. Today* **2014**, *230*, 131–137.  
30  
31  
32  
33  
34 (51) Orendorff, C. J.; Sau, T. K.; Murphy, C. J. Shape-Dependent Plasmon-Resonant  
35 Gold Nanoparticles. *Small Weinh. Bergstr. Ger.* **2006**, *2*, 636–639.  
36  
37  
38  
39 (52) Marschall, R. Semiconductor Composites: Strategies for Enhancing Charge Carrier  
40 Separation to Improve Photocatalytic Activity. *Adv. Funct. Mater.* **2014**, *24*, 2421–2440.  
41  
42  
43  
44 (53) Ge, Y.; Shah, Z. H.; Wang, C.; Wang, J.; Mao, W.; Zhang, S.; Lu, R. In Situ  
45 Encapsulation of Ultrasmall CuO Quantum Dots with Controlled Band-Gap and Reversible  
46 Thermo-chromism. *ACS Appl. Mater. Interfaces* **2015**, *7*, 26437–26444.  
47  
48  
49  
50  
51  
52  
53  
54  
55  
56  
57  
58  
59  
60

TOC graphic

